

Numerical estimation of the escaping flux of massless particles created in collisions around a Kerr black hole

Andrew J. Williams^{1,2,*}

¹Royal Holloway, University of London, Egham, TW20 0EX, UK

²Rutherford Appleton Laboratory, Chilton, Didcot, OX11 0QX, UK

(Dated: May 25, 2022)

The geodesics of massless particles produced in collisions near a rotating black hole are solved numerically and a Monte Carlo integration of the momentum distribution of the massless particles is performed to calculate the fraction of massless particles that escape the black hole to infinity. A distribution of in falling dark matter particles, which are assumed to annihilate to massless particles, is considered and an estimate of the emergent flux from the collisions is made. The total flux and the energy spectrum of the massless particles is calculated. The shape of the spectrum is found to depend on the density profile of the dark matter and could provide information about the size of the annihilation plateau around a black hole and the mass of the dark matter particle.

PACS numbers: 97.60.Lf, 04.70.-s, 95.35.+d

I. INTRODUCTION

Intermediate mass black holes may be associated with a density spike of dark matter [1] that can provide an enhancement in the annihilation of dark matter particles to gamma rays or neutrinos. The indirect detection of dark matter through its annihilations could provide information about the nature of the dark matter in the galaxy and its distribution. The physics of particle collisions in the gravitational field of a black hole has been extensively studied, see e.g. [2] [3] [4] [5] [6] [7] [8] [9] [10]. In the case of rotating black holes collisions between dark matter particles can yield large centre of mass energies [3] and inside the ergosphere particles produced via the Penrose process could carry high energies [6]. In order to make use of any such collisions around a black hole it will be important to understand the fate of the particles produced, in particular the fraction of particles produced that escape the black hole compared to those which cross the event horizon. The escape fraction can be defined as the fraction of particles that escape from a collision between two dark matter particles and depends on the momenta of the dark matter particles and the distance from the black hole. The escape fraction has been calculated for maximally rotating black holes where massless particles are emitted in the equatorial plane of the black hole [11] and is also known for Schwarzschild black holes [12]. However a general analytical solution is not known for rotating black holes where the particles can be emitted in all directions.

The goal of this paper is to find a numerical result for the escape fraction of massless particles produced in collisions around a rotating black hole and to investigate the energy spectrum of any emergent flux. We assume an interaction of the form $\chi\chi \rightarrow xx$ where x is a massless

particle that could be a photon or neutrino. To simplify the analysis, we assume that the final state particles are emitted isotropically in the centre of mass frame of the collision. We will concentrate on investigating the general shape of the energy spectrum without worrying about the exact value of the flux expected from a particular black hole.

The paper is organised as follows: in Section II the method of numerically solving the geodesic equation for a massless particle in a Kerr metric with arbitrary rotation is presented. Section III uses this to obtain the escape fraction for massless particles and introduces the effect of a boosted frame of reference due to the momentum of the colliding particles. In Section IV the physics of the particles created in such collisions is investigated with respect to the role of centre of mass energy and the Penrose process in shifting the spectrum of emergent massless particles. Section V presents the spectrum of emergent particles from the collisions and how the dark matter density distribution dictates the shape of the spectrum. In Section VI we present our conclusions.

II. NUMERICAL SOLUTION OF THE GEODESIC EQUATION

To know whether a particular massless particle escapes the black hole or not its geodesic equation must be solved and the behaviour as $t \rightarrow \infty$ found. This is most easily performed using Boyer-Lindquist coordinates as defined in Ref. [13]. In these coordinates the metric for a Kerr black hole has the form [13],

$$ds^2 = - \left(1 - \frac{2Mr}{\Sigma} \right) dt^2 - \left(\frac{4Mar \sin^2 \theta}{\Sigma} \right) dt d\phi + \frac{\Sigma}{\Delta} dr^2 + \Sigma d\theta^2 + \left(r^2 + a^2 + \frac{2Ma^2 r \sin^2 \theta}{\Sigma} \right) \sin^2 \theta d\phi^2, \quad (1)$$

*Electronic address: williams@pheno.pp.rhul.ac.uk

where M is the mass of the black hole, a is the angular momentum per unit mass of the black hole and the following functions are defined [13],

$$\Delta \equiv r^2 - 2Mr + a^2, \quad (2)$$

$$\Sigma \equiv r^2 + a^2 \cos^2 \theta. \quad (3)$$

For simplicity the mass of the black hole is set to $M = 1$ as a result the angular momentum of the black hole, a , ranges between 0 and 1. The units were set as $r_s = \frac{M_{BH} G}{c^2} = 1$. The trajectories of a particle are then defined by 3 constants of motion which are conserved, the forms of these quantities are [13]

$$\begin{aligned} E &= -p_t, & L &= p_\phi, \\ Q &= p_\theta^2 + \cos^2 \theta \left(a^2 (\mu^2 - p_t^2) + \frac{p_\phi^2}{\sin^2 \theta} \right). \end{aligned} \quad (4)$$

Here μ is the mass of the particle, E is the energy, L is the component of the angular momentum parallel to symmetry axis of the black hole and $Q + p_\phi^2$ is the total angular momentum squared when $a = 0$ but receives corrections for Kerr black holes. Q characterises the motion in the θ direction and for $Q = 0$ particles in the equatorial plane will remain restricted to that plane [13]. The equations of motion for the particles can now be written in terms of λ , which will become an affine parameter for massless particles, and are written here in the form given by Ref. [13],

$$\begin{aligned} \Sigma \frac{dr}{d\lambda} &= \pm V_r = \pm \sqrt{T^2 - \Delta \left(\mu^2 r^2 + (L - aE)^2 + Q \right)}, \\ \Sigma \frac{d\theta}{d\lambda} &= \pm V_\theta = \pm \sqrt{Q - \cos^2 \theta \left(a^2 (\mu^2 - E^2) + \frac{L^2}{\sin^2 \theta} \right)}, \\ T &= E(r^2 + a^2) - La. \end{aligned} \quad (5)$$

The final state particles of the collisions will be assumed to be massless allowing the equations to be simplified by setting $\mu = 0$. We will be interested in the r and θ behaviour. The effective potentials V_r and V_θ are fully separated and are functions of only r and θ respectively. The coupling between θ and r is encoded in the Σ factor in the equations of motion. Both t and ϕ do not enter in the equations for r or θ so there is no need to solve for their behaviour. Instead $r(\lambda)$ and $\theta(\lambda)$ will be found numerically. In order to calculate the escape function numerically there needs to be a way to check whether a massless particle emitted in a particular direction at a position r_0 will escape or if it will cross the event horizon. To do this the equations of motion for r and θ were integrated by a Runge-Kutta method until the massless particle either crossed the horizon or escaped to some large value of r . The algorithm employed was based on an embedded adaptive step size Runge-Kutta formula as outlined in Ref. [14]. The equation of motion for the r coordinate has 2 solutions with opposite signs corresponding to massless particles travelling towards or away from

the black hole, the sign is chosen based on the initial conditions and turning points in the r solution must be detected and the sign changed. A numerical check was used to determine when the derivative of r became very small, when this occurs the sign of the r solution was changed.

The integration was ended whenever the massless particle crossed the horizon or achieved some maximum distance from the black hole, $r_{max} \approx 100$ for collisions close to the horizon and was increased as r_0 increased. In some cases the massless particle remained bound by the black hole in a stable orbit in this situation the integration would end only when some maximum value of λ was reached. If λ_{max} is set too high then solutions with several turning points are computationally intensive. However setting a low value of λ_{max} is not suitable since some escaping massless particles do so only after a long time. The integration for these can be rapid since the step size can be large and therefore the actual number of integration steps small. To avoid these problems bound orbits were detected by tracking the number of turning points encountered by a solution when this became large, more than 100, the massless particle was assumed to be trapped and the integration ended. In practise the parameters of the algorithm, the minimum step size, λ_{max} , r_{max} and the value of $\frac{dr}{d\lambda}$ that indicates a turning point were varied to find optimal values that did not introduce errors in the final result by checking with test cases and known analytical solutions where available.

III. THE ESCAPE FRACTION

This method for solving the geodesic equation for the massless particle then allows the escape fraction of massless particles produced in collisions around the black hole to be calculated. The escape fraction was calculated by a Monte Carlo integration over the final momentum of the produced massless particle pair. In the centre of mass frame of the colliding particles the massless particles are emitted back to back and carry energy equal to one half of the centre of mass collision energy. The momentum integration is therefore reduced to an integration over two angles θ and ϕ as the angles from the radial direction. For the integration only one of the pair of massless particles was considered and a flat distribution of the angles was generated. For each generated direction the geodesic equation was solved numerically as above and the massless particle was recorded as either escaping or becoming trapped by the black hole. The escape fraction was then taken as the number of massless particles recorded as escaping divided by the total number generated.

The uncertainty in the escape fraction due to the statistical effects of the Monte Carlo integration were calculated by separating the massless particles into discrete bins, the escape fraction for each bin was calculated then the average escape fraction taken. The variance in the escape fraction calculated for each bin then gave an esti-

mate for the uncertainty in the averaged escape fraction. This uncertainty does not account for any error in the numerical solution for the geodesic equations but since the escape fraction only depends on the general behaviour of each massless particle this was ignored.

To test the implementation of the numerical method the escape function can be calculated for the $a = 0$ Schwarzschild case. Analytically the escape function for this case is known [12]. Fig. 1 shows the behaviour of the

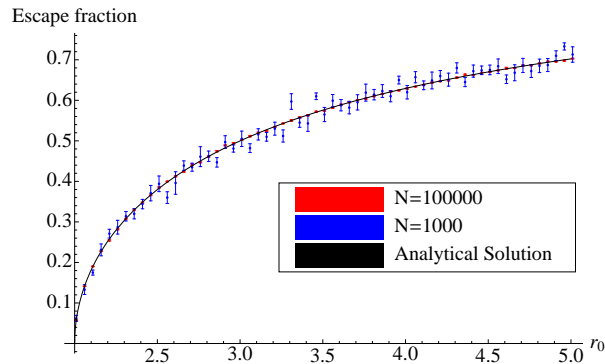


FIG. 1: The escape fraction for $a = 0$, where N is the number of Monte Carlo iterations

escape fraction when the massless particle is emitted in an unboosted frame so that the emission is isotropic in the lab frame. The escape fraction matches the analytical solution [12] with some variation due to the Monte Carlo integration. The effect of the number of Monte Carlo iterations on the error in the escape fraction can be seen and gives an indication of the number of iterations required to give a good agreement with the analytical solution.

A. Locally non-rotating and boosted frames

Having tested the machinery for the non-rotating case results can be obtained for black holes with $a > 0$. For $a = 1$ it will be useful to consider two cases for the numerical calculation, firstly where the massless particles are generated with no component of their motion outside the equatorial plane ($Q = 0$) and secondly where they are generated in all directions to compare with the result found in [11]. For a rotating black hole there is another complication. So far the massless particles have been assumed to be emitted in a locally flat frame that is at rest in the Boyer-Lindquist coordinate system. For a rotating black hole the corresponding frame is that of a locally non rotating frame (LNRF) [13]. A LNRF represents a set of Minkowski coordinates such that the physics in this local frame can be described by special relativity. This is further complicated when the centre of mass frame of the collision is Lorentz boosted relative to the LNRF. In this case it is easiest to generate the massless particle momentum in the centre of mass frame where it is assumed to be isotropic and apply a Lorentz transformation at attain

the momentum in the LNRF.

The goal is to transform a Monte Carlo generated isotropic distribution of massless particle directions in the centre of mass frame into a distribution of the constants of motion in the Boyer-Lindquist coordinate system so that the geodesic equation can be solved. The transformation between the two will in general be a function of r_0 and θ_0 coordinates at which the collision takes place and $\Lambda(P, Q)$ the Lorentz transformation between the centre of mass frame and the LNRF where P and Q are the momenta of the colliding particles. For details on transforming between a LNRF and a Boyer-Lindquist system see Ref. [13], while the method of calculating $\Lambda(P, Q)$ we follow that in Ref. [11].

The general procedure for the calculation of the massless particle momentum in the Boyer-Lindquist coordinates was carried out as follows. Firstly the momentum of the incoming particles was defined in the Boyer-Lindquist frame by setting the constants of motion and evaluating the equation for their momentum at the coordinates that the collision was assumed to take place. The incoming momenta were transformed to the locally non-rotating frame. With the two momenta of the incoming particles defined in this locally flat space the relative momentum of the centre of mass frame was found and the boost between these two frames calculated. The massless particle direction was then randomly generated in the centre of mass frame, the boost between the locally non-rotating frame and the centre of mass frame was inverted to allow the massless particle momentum in the locally non-rotating frame to be calculated. Finally the massless particle momentum in the Boyer-Lindquist coordinates was calculated and the constants of motion for the massless particle found. The geodesic equation for the massless particle could then be integrated as before.

The momentum of the incoming particles was calculated following the procedure in Ref. [11] which calculated the velocities of the incoming particles for particles restricted to the equatorial plane. The momenta of the two incoming particles was then used to produce the 4 dimensional Lorentz boost matrix between the LNRF and centre of mass frame. Fig. 2 shows the escape fraction as a function of r for collisions between falling particles with angular momentum $l_1 = 2$, $l_2 = -2$ for $a = 1$ in the equatorial plane. The analytical solution [11] when restricted to the equatorial plane is also shown. The numerical result matches the exact solution in the equatorial plane and the numerical result for emission in all directions is comparable.

IV. DISTRIBUTIONS OF INCOMING AND OUTGOING MOMENTUM

The previous section considered massless particles produced in collisions from particles with fixed incoming momenta however the escape fraction depends on the Lorentz boost from the LNRF to the centre of mass frame

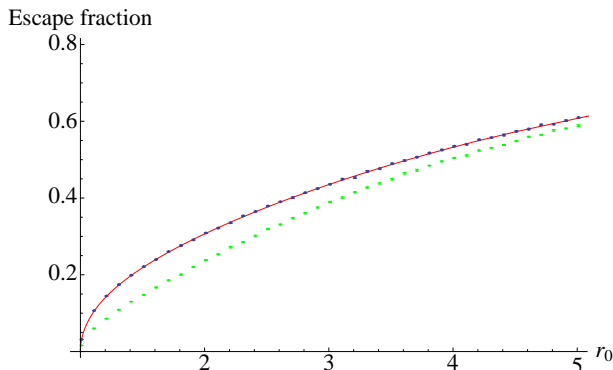


FIG. 2: Escape fraction for $a=1$: Analytic solution in equatorial plane (red line) [11], Numerical result in equatorial plane (blue points) and full numerical result allowing propagation in all directions (green points).

given above and is derived from the constants of motion E , L , Q in the Boyer-Lindquist coordinates of the incoming particles. These constants are not fixed in general and the momenta of the colliding particles will have some distribution. This distribution will also effect the centre of mass energy of the collision and the energy of the produced massless particles as well as the direction in which they are emitted. In order to calculate the energy distribution of escaping particles and the general escape fraction it will therefore be important to consider incoming particles with some distribution of momenta.

The form of this distribution is not known so we instead assume a flat distribution in the constants L and Q . The allowed range of L and Q was fixed by considering only particles with geodesics that would allow the particle to fall from some large r to the radius r_0 at which the collision takes place. The constant of motion E was set to 1, the mass of the dark matter. The range of allowed constants of motion was calculated by fixing θ to the equatorial plane then calculating $\frac{dr}{d\lambda}$ as a function of r starting at $r \gg r_0$ then running down in small steps of r to the value r_0 , if $\frac{dr}{d\lambda}$ becomes very small then we assume that a turning point is reached and that a particle could not fall from infinity to r_0 . The distribution was sampled by Monte Carlo integration. So that for each massless particle generated to calculate the escape fraction a pair of incoming momenta was chosen with a random L and Q . Figure. 3 shows the allowed range in L and Q for collisions occurring at $r_0 = 1.1$ as an example. This is characterised (for $a = 1$) by a maximum value of Q which occurs for $L = -1$ as well as a maximum and minimum value of L with the largest range corresponding to $Q = 0$. In practise for each value of r the maximum value of Q was found along with L_{min} and L_{max} evaluated for $Q = 0$ and random values in the region $L_{min} < L < L_{max}$ and $Q < Q_{max}$ were generated and specific combinations of L and Q checked to make sure that the particle could indeed reach r_0 . Figure. 4 shows the escape fraction when the momenta of the colliding particles is integrated over all allowed values of L

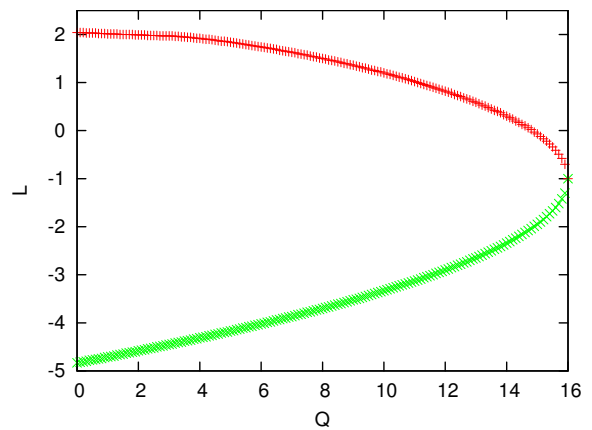


FIG. 3: Allowed range in Q and L for incoming particles at $r = 1.1$ with $a = 1$. The red line show L_{max} and the green line L_{min} .

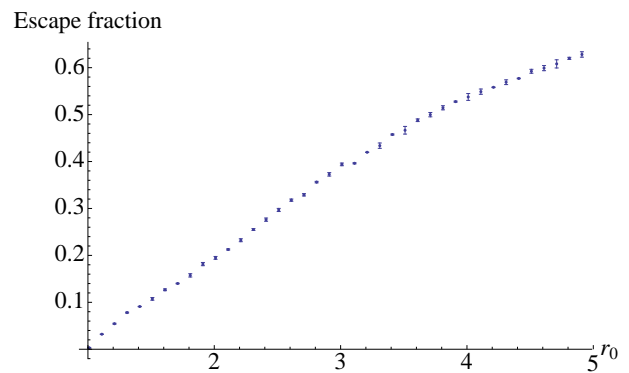


FIG. 4: Escape fraction with integration over allowed incoming momenta.

and Q . The escape fraction has only a weak dependence on the Lorentz boost of the colliding particles so the full escape fraction is only a slight shift from the result found for a particular fixed boost.

Having generated massless particles from distribution of colliding particles the spectrum of the annihilation products can now be investigated. The energy measured at infinity is equal to the constant E in the Boyer-Lindquist system so the energies of produced massless particles can be found directly.

There are 4 processes that will effect the energy of the annihilation products, the centre of mass energy of the collision, the gravitational red shift, the Lorentz boost between centre of mass frame and the LNRF and finally the effects from the rotation of the black hole and direction of the emitted massless particle coming from the transformation between the LNRF and Boyer-Lindquist coordinate system.

Fig. 5(a) shows the spectrum, in units of the dark matter mass, of massless particles produced in the collision. This spectrum is for the unrealistic case that every parti-

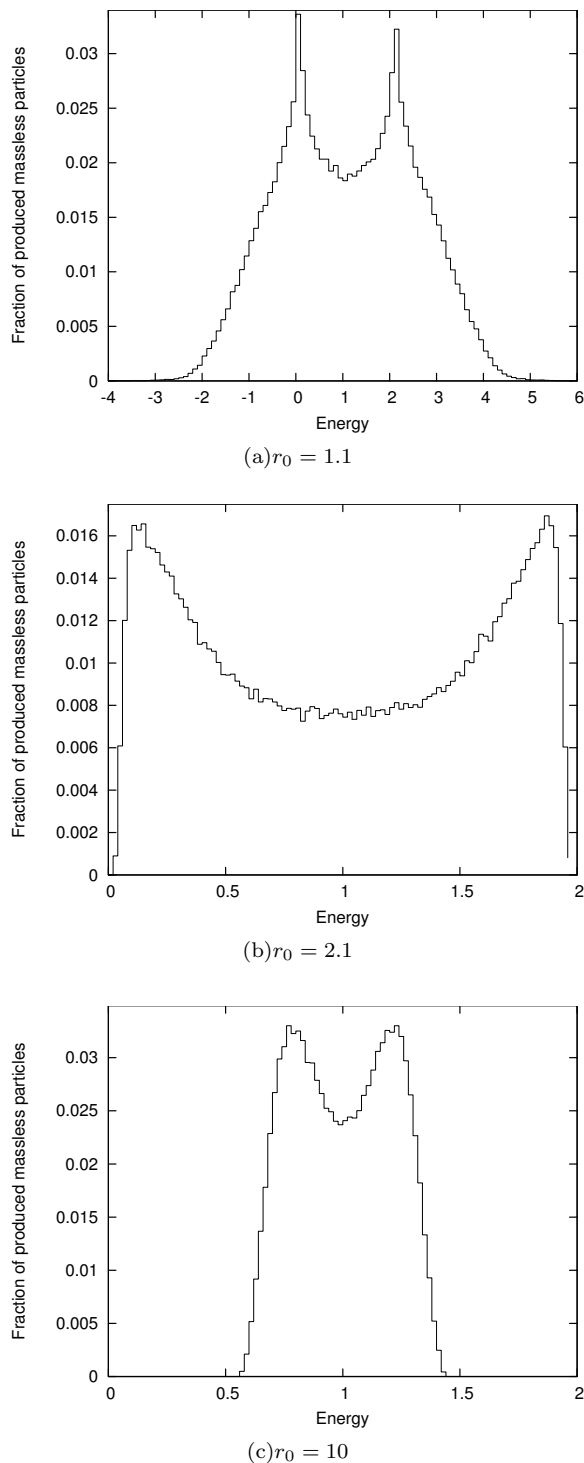


FIG. 5: Energy spectrum at infinity of massless particles produced in collisions at varying r_0 if all the particles were “allowed to escape”. ($a = 1$)

cle produced is allowed to escape and its energy measured at infinity. The first thing to note is that the energy spectrum of the massless particles contains a peak around the order of the dark matter mass for all r_0 due to the balance between the gravitational red shift and centre of mass

energy. For $r_0 < 2$ inside the ergosphere the spectrum has two peaks centred around $E = 0$ and $E = 2$. This can be explained by the Lorentz boost, in both the lab frame and L NRF the two colliding dark matter particles are in general travelling towards the black hole. From these frames the centre of mass frame of the collision appears to be Lorentz boosted towards the black hole in the radial direction. For most of the combinations of incoming momenta of the dark matter this boost in the radial direction is much larger than the boosts in the θ and ϕ directions. The Lorentz boost in the radial direction then causes the collision to appear to an observer at large r as a source of massless particles travelling towards the black hole and away from the observer. A particle emitted in the positive radial direction therefore appears red shifted to the observer. The massless particles emitted towards the event horizon are blue shifted as can be seen from conservation of energy in the observers frame or from considering an observer located on the opposite side of the black hole for whom the collision frame is boosted towards them. For some values of L and Q the massless particles emitted towards the black hole undergo a reflection in the radial direction and can then escape to infinity and be detected. Close to the black hole where the Lorentz boost between the L NRF and centre of mass frame is largest the red shifted photon will carry close to zero energy while the blue shifted photon will carry nearly all the energy from the collision. Transforming from the L NRF to the Boyer-Lindquist coordinates the total energy of the collision is $E = 2$ and so the spectrum is made up of massless particles with $E \approx 0$ and $E \approx 2$. However for $r_0 < 2$ it can be seen that the peaks extend to $E > 2$ and $E < 0$ due to the Penrose process see [6] and [15]. For massless particles produced in pairs in the centre of mass frame the $E < 0$ and $E > 2$ lie in opposite directions such that the total energy of the system of massless particles is always 2.

For $r_0 > 2$ (Figure. 5(b)) the Penrose process no longer occurs so massless particle energies are limited to $0 < E < 2$. Close to $r_0 \gtrsim 2$ the Lorentz boost is still large and the spectrum is dominated by peaks at $E \approx 0$ and $E \approx 2$ and then as the radius at which the collision occurs, r_0 , increases further the momentum of the dark matter particles in the radial direction decreases and so the effect of the Lorentz boost gets smaller and these two peaks move inwards and bunch more tightly around $E = 1$ (Figure. 5(c)).

V. SPECTRUM OF EMERGENT MASSLESS PARTICLES

We know from the calculation of the escape fraction that not all massless particles produced in the collisions will escape and so the observed spectrum will differ from that found above. The escape fraction should depend on the energy of the massless particles, this clearly must be the case since we already know that no negative en-

ergy massless particles can escape the ergosphere. The final spectrum of massless particles observed far from the black hole will then be a convolution of the spectrum produced in the collisions and the energy dependent escape fraction.

The shape of the spectrum of escaping massless particles can be seen in Figure. 6 which shows the fraction of escaped massless particles found in each energy bin. Comparing Figure. 6(a) and Figure. 5(a) the effect of the escape fraction on the spectrum of massless particles can be seen. The emergent spectrum contains only one peak corresponding to the low energy peak in Figure. 5(a) the second peak has been cut off by an escape fraction which favours lower energy massless particles since these are emitted away from the black hole initially. This has the effect of greatly reducing the chance to observe the high energy massless particles created via the Penrose process despite the greater abundance of such massless particles in the initially produced spectrum. It is also the case that there are no negative energy massless particles escaping to infinity which is as expected.

Figure. 6(b) shows the spectrum of escaping massless particles for collisions at $r_0 = 2.1$ the shape of the spectrum changes due to the shifting inwards of the boosted peaks in the produced spectrum and also the larger escape fraction. As the escape fraction allows more energetic massless particles to escape the spectrum develops a flattened tail extending towards higher energies where the decreasing escape fraction and increasing production of massless particles are balanced.

Figure. 6(c) shows the spectrum for collisions much further from the the black hole, here the escape fraction is approaching one and the spectrum of escaping massless particles looks more like the initially produced spectrum with two peaks. There is still a slight bias towards the initially outgoing massless particles such that the heights of the two peaks are not equal as r_0 increases further the escape fraction will become less important and the spectrum will eventually approximate the spectrum of massless particles produced in the collisions.

In order to calculate the spectrum that would be observed we must integrate the effect of collisions over the volume of dark matter surrounding the black hole. The method of calculation of the flux follows [11] using the result for the flux arriving at some distance D

$$\Phi \approx \frac{\sigma v R_s^3}{4\pi m_\chi^2 D^2} \int_{r_h}^{r_\infty} \rho^2(r) e(r) dV, \quad (6)$$

where σv is the cross-section for annihilation to massless particles which we assume to be energy independent, m_χ is the mass of the dark matter particles, R_s is the Schwarzschild radius, $e(r)$ is the escape fraction and $\rho(r)$ is the dark matter density around the black hole. It is assumed that the density distribution of dark matter and the escape fraction are spherically symmetric. By writing

$$\rho(r) = \rho_{pl} \rho_0(r), \quad (7)$$

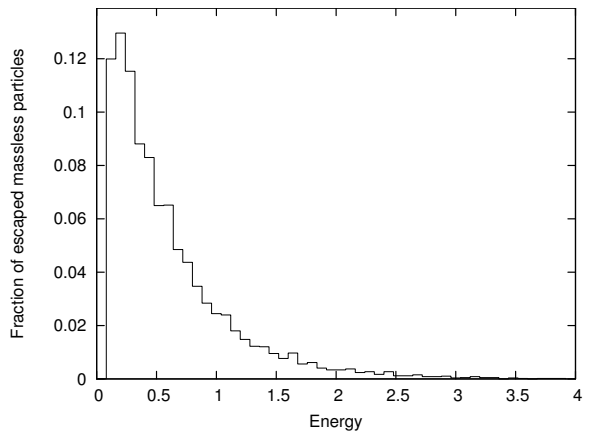
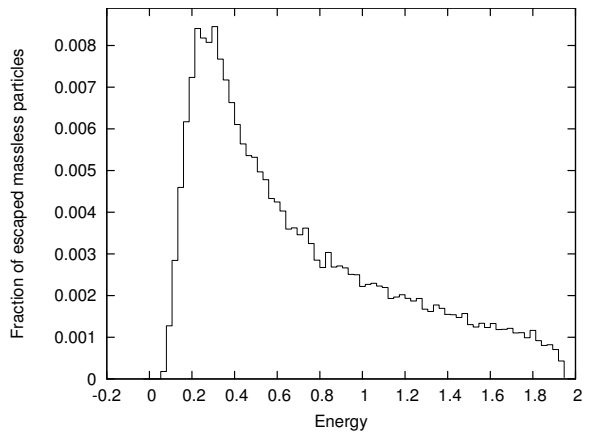
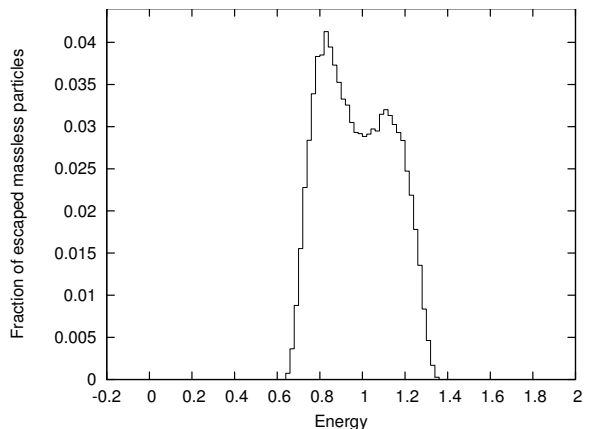
(a) $r_0 = 1.1$ (b) $r_0 = 2.1$ (c) $r_0 = 15$

FIG. 6: Spectrum of escaping massless particles produced at varying r_0 . The fraction of massless particles that escape the black hole with energy in each bin normalised to the total number of particles produced. ($a = 1$)

where $\rho_0(r)$ is a dimensionless function giving the shape of the density profile the flux can be written in terms of a dimensionless integral containing all the of the dependence on the rotation of the black hole and the shape

density profile as [11],

$$\Phi \approx \frac{\sigma v R_s^3 \rho_{pl}}{m_\chi^2 D^2} \mathcal{I}(a, r_1), \quad (8)$$

$$\mathcal{I}(a, r_1) = \int_{r_h}^{r_1} r^2 \rho_0^2(r) e(r) dr, \quad (9)$$

where r_1 is some cut off to the integration which should go to infinity to give the total flux. In order to calculate the spectrum of the emergent massless particles we need to know $\Phi(E)$ which depends on the convolution of the escape fraction and spectrum of produced massless particles. To find this $p(r, E_1, E_2)$ was defined as the fraction of massless particles that escape with energy $E_1 < E < E_2$ per collision. This was found numerically by simply separating the escaped massless particles into bins of energy and dividing by the total number of Monte Carlo iterations. It can be seen that summing over all of the energy bins then gives the total escape fraction $e(r)$. The integral can then be rewritten as

$$\Phi(E_1, E_2) \propto \mathcal{I}(a, r_1, E_1, E_2) = \int_{r_h}^{r_1} r^2 \rho_0^2(r) p(r, E_1, E_2) dr, \quad (10)$$

where summing over all the energy bins gives the total flux.

The density distribution of dark matter around black holes has been extensively studied see [1] [16] [17]. Considering the case of an intermediate mass black hole the density distribution can be described as follows [1], close to the black hole there is an annihilation plateau with constant density $\rho_{pl} = m_\chi/(\sigma v t)$ where t is the formation time of the black hole. This holds out to a radius r_{cut} from which point the density falls off with a power law $\rho \propto r^{-\frac{7}{3}}$. The flux should be dominated by contributions from the annihilation plateau and density spike since the escape fraction is only small for the radii much smaller than the annihilation plateau so the distribution much further from the black hole will not be of interest. It is now clear that if ρ_{pl} given in Eq. 7 is taken to be the density of the annihilation plateau, $\rho_0(r)$ will take the form [1],

$$\rho_0(r) = \begin{cases} 1 & \text{if } r < r_{cut} \\ \left(\frac{r}{r_{cut}}\right)^{-\frac{7}{3}} & \text{if } r > r_{cut} \end{cases}. \quad (11)$$

Since the escape fraction is increasing with r the integrand in \mathcal{I} will increase with r up to r_{cut} at which point the falling density means that the integrand gets smaller as a function of r so that the contributions to \mathcal{I} from collisions with $r_0 > r_{cut}$ get smaller as r_0 increases. The flux will therefore be dominated by the collisions in the region of r_{cut} where we have the maximum of the product $r^2 \rho_0^2(r) p(r, E_1, E_2)$. This holds generally for distributions of this form so long as the density distribution drops off faster than $1/r^2$. The integration should therefore be continued up to some value of r where the relative

contribution of each succeeding shell of the numerical integration is small. In practise it was possible to continue until new contributions to \mathcal{I} were less than 0.1% of the total.

To calculate the value of \mathcal{I} for a particular set of black hole parameters the value of r_{cut} needs to be specified. In general this depends on the mass of the black hole and on the annihilation cross-section of the dark matter. For the super massive black hole at the centre of the galaxy this was estimated to be $r_{cut} \approx 10^{-4.4} pc = 4 \times 10^{-5} pc$ from Ref. [16] which is $r_{cut} = 137 r_{Sch}$ in terms of the Schwarzschild radius.

The exact value is not important since the shape of the spectrum remains distinctive over a large range of r_{cut} and a measurement of the spectrum should in principle allow r_{cut} to be determined. To show this, the spectrum produced for a number of different values of r_{cut} are shown in Figure. 7.

Figure. 7(a) shows the spectrum for a small value of r_{cut} here the spectrum is characterised by a single asymmetric peak bellow the dark matter mass. The peak itself is broad and the mass of the dark matter is found to be roughly equidistant from the peak and the edge of the shoulder in the distribution. As r_{cut} increases both peaks become clearly visible and the spectrum becomes less broad. The height difference between the peaks also decreases as they get closer together. The dark matter mass is indicated by the minimum between the peaks and the value of r_{cut} can be estimated from the separation of the peaks as a fraction of the dark matter mass.

The value of r_{cut} can be estimated as follows, the dark matter mass must be found first by locating the minimum of the spectrum the energy at which the first peak occurs as a fraction of the mass of the dark matter then decreases as a function of r_{cut} . By plotting the peak location as a function of r_{cut} from simulation the expected value of r_{cut} can be found for a given peak separation. It should be noted that the distribution is not exactly symmetric and that the higher energy peak is located closer to the dark matter mass than the lower energy peak. However both could be used to find an estimate of r_{cut} and the ratio of the height of the peaks could also be utilised in this way. One problem with this analysis is that it assumes that the angular momentum of the black hole is known and varying a shifts the separation of the peaks, however this effect is much smaller than changing r_{cut} but would still introduce uncertainty in the estimation. The ability to resolve the peaks depends on the total flux available and the energy resolution around the dark matter mass of a particular measurement, in terms of the annihilation plateau the separation of the peaks was found up to $r_{cut} = 10^5 R_s$ with a separation of $\Delta_E \sim 0.005 m_\chi$ and $\Delta_E \sim 0.1 m_\chi$ for $r_{cut} = 10^3 R_s$. In the case that the peaks can not be resolved then the spectrum can be approximated as a single peak with a width comparable to the peak separation centred at the dark matter mass.

The total flux can be estimated by choosing some suitable values for the parameters in Eq. 9. Setting the mass

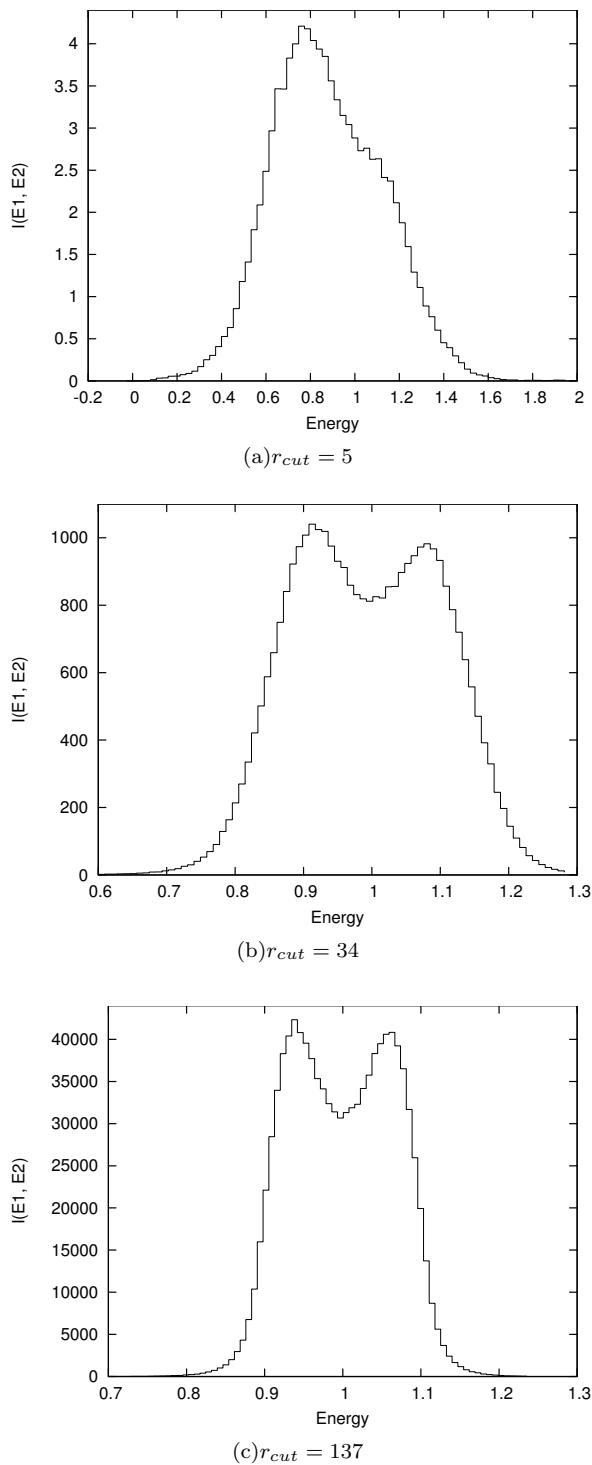


FIG. 7: Spectrum of massless particles escaping to infinity with a cut off in dark matter density at various values of r_{cut} . ($a = 1$)

of the black hole to $M = 40 \times 10^5 M_\odot$, the annihilation cross-section of the dark matter as $\langle\sigma v\rangle = 10^{-28} \text{cm}^2 \text{s}^{-1}$, the distance from the black hole $D = 10 \text{pc}$ and the time-scale for the growth of the black hole as $t_0 = 10^{10} \text{years}$

gives a total flux of [11],

$$\Phi = \Phi_0 \mathcal{I}, \quad (12)$$

where $\Phi_0 = 3.41 \text{km}^{-2} \text{year}^{-1}$. Integrating from $r_0 = 1$ to $r_0 = 300$ for $r_{cut} = 137$ gives a total value of $\mathcal{I} \approx 10^6$ which gives a total flux of $\Phi \approx 3 \times 10^6 \text{km}^{-2} \text{year}^{-1}$.

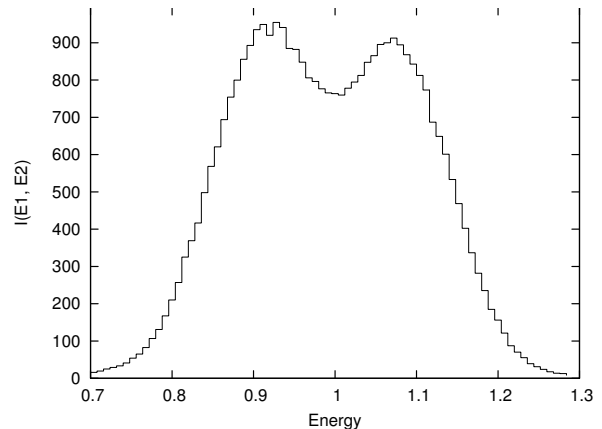


FIG. 8: $\mathcal{I}(r_{cut} = 34, E_1, E_2)$ for $a = 0$

The shape of the spectrum can also be considered for a non-rotating black hole and for a reasonable value of r_{cut} gives a flux very similar to the Kerr case. Figure. 8 shows the spectrum for a non-rotating black hole with $r_{cut} = 34$ and differs from Figure. 7(b) by having a slightly larger flux and the peaks closer to $E = 1$. This is due to the smaller Lorentz boosts associated with the Schwarzschild black hole and a faster growing escape fraction. This is found in contrast to the spectrum in Ref. [2] where the spectrum was found to have a narrow single peak. In considering the incoming dark matter particles to have momenta distributed over the whole range of allowed in falling geodesics the Lorentz shifting of the peak is found to have a splitting effect giving rise to two peaks that accounts for this difference.

VI. CONCLUSIONS

In conclusion we have shown that annihilation of dark matter to massless particles around a black hole can produce a distinctive signal independent of the particle model. The spectrum is found to be centred around the dark matter mass with splitting to two peaks due to the Lorentz boosting of the centre of mass frame of the colliding particles. The shape of the spectrum retains its distinctive shape when integrated over a typical density profile for the dark matter and can in fact reveal details of the distribution in particular the radius of the annihilation plateau thought to occur. The shape of the spectrum is not dependent on the total flux of massless particles from the annihilations which depends on several

unknown parameters for a particular source and is therefore a useful tool in discriminating such a signal from astrophysical backgrounds.

In calculating the energy spectrum we assumed that the annihilation cross-section of the dark matter was independent of the centre of mass energy, for a particular dark matter model the energy dependence of the cross section could change the shape of the spectrum since the centre of mass energy depends on the distance from the black hole at which the collision occurs. The size of this effect can be approximated by considering the ratio between the maximal cross-section σ_{max} and the cross-section at r_{cut} , which we call σ_{cut} , the ratio is then $\sigma_{\Delta} = \frac{\sigma_{max}}{\sigma_{cut}}$. This ratio should then be compared to the ratio of the product $\tilde{\rho}(r) = r^2 \rho_0^2(r) p(r)$ evaluated at r_{cut} and the value at r for which the cross-section is largest, defined as $\tilde{\rho}_{\Delta} = \frac{\tilde{\rho}(r_{cut})}{\tilde{\rho}(r_{\sigma_{max}})}$. If $\tilde{\rho}_{\Delta}$ is much larger than σ_{Δ} then the contribution to the flux from collisions around r_{cut} will still dominate. If σ_{Δ} is larger then the spectrum will be dominated by collisions occurring at r where the cross-section is at its maximum. This approximation ignores the dependence of the Lorentz boost on the centre of mass energy and assumes that the cross-section can be averaged as a function of r_0 . To fully understand the effect of an energy dependent cross-section a more detailed analysis of the resulting spectrum would need to be performed which we leave for future work.

In the numerical analysis carried out the collisions were assumed to occur on the equatorial plane and in reality the collisions occurring outside of the equatorial plane could change the shape of the total spectrum. However

the results have been checked for collisions at $\theta = 0.6$ for $r_{cut} = 34$ and the spectrum retains the same structure with a lower total flux but the same separation between peaks. It would therefore appear that the radial dependence of the energy spectrum dominates over any θ dependence. For small r the spectrum will differ due to the dependence of the radius of the ergosphere on θ however for reasonable value of r_{cut} the spectrum is dominated by collisions far beyond the ergosphere.

The results also demonstrate that while large centre of mass energies are possible in collisions close to the horizon the emitted massless particles will in general be largely red shifted to energies below the dark matter mass. The detection of such particles may then rely on the energy dependence of the cross section. Other high energy massless particles were found in the spectrum with energies far larger than the dark matter mass due to the Penrose process, the non-zero escape fraction for these particles means that collisions around black holes could still be a source of energetic photons or neutrinos with energies several times the dark matter mass.

VII. ACKNOWLEDGEMENTS

We thank Joseph Silk and Stephen West for useful discussions. This work was supported by the Higher Education Funding Council for England and the Science and Technology Facilities Council under the SEPNet Initiative.

-
- [1] G. Bertone, M. Fornasa, M. Taoso and A. R. Zentner, *New J. Phys.* **11** (2009) 105016 [arXiv:0905.4736 [astro-ph.HE]].
 - [2] A. N. Baushev. Dark matter annihilation in the gravitational field of a black hole, arXiv:0805.0124 [astro-ph] 2008
 - [3] M. Banados, J. Silk and S. M. West, *Phys. Rev. Lett.* **103**, 111102 (2009) [arXiv:0909.0169 [hep-ph]].
 - [4] E. Berti, V. Cardoso, L. Gualtieri, F. Pretorius and U. Sperhake, *Phys. Rev. Lett.* **103** (2009) 239001 [arXiv:0911.2243 [gr-qc]].
 - [5] T. Jacobson and T. P. Sotiriou, *Phys. Rev. Lett.* **104** (2010) 021101 [arXiv:0911.3363 [gr-qc]].
 - [6] A. A. Grib and Yu. V. Pavlov, arXiv:1001.0756 [gr-qc].
 - [7] S. W. Wei, Y. X. Liu, H. Guo and C. E. Fu, *Phys. Rev. D* **82** (2010) 103005 [arXiv:1006.1056 [hep-th]].
 - [8] O. B. Zaslavskii, *Phys. Rev. D* **82** (2010) 083004 [arXiv:1007.3678 [gr-qc]].
 - [9] T. Harada and M. Kimura, *Phys. Rev. D* **83** (2011) 024002 [arXiv:1010.0962 [gr-qc]].
 - [10] M. Kimura, K. i. Nakao, H. Tagoshi, [arXiv:1010.5438 [gr-qc]].
 - [11] M. Banados, B. Hassanain, J. Silk and S. M. West, arXiv:1010.2724 [astro-ph] 2010
 - [12] Charles W. Misner, Kip S. Thorne, John A. Wheeler, *Gravitation*, W. H. Freeman; 2nd Printing edition (1973)
 - [13] James M. Bardeen, William H. Press, and Saul A Teukolsky. Rotating black holes: Locally nonrotating frames, energy extraction, and scalar synchrotron radiation. *Astrophys. J.*, 178:347, 1972.
 - [14] Press, Williams H. Numerical recipes in C: The art of scientific computing. Cambridge University Press, 2002
 - [15] J. Gariel, M. A. H. MacCallum, G. Marcilhacy and N. O. Santos. Kerr geodesics, the Penrose process and jet collimation by a black hole, *Astronomy & Astrophysics* 515, A15 2010
 - [16] G. Bertone and D. Merritt, *Mod. Phys. Lett. A* **20** (2005) 1021 [arXiv:astro-ph/0504422].
 - [17] G. Bertone, A. R. Zentner and J. Silk, *Phys. Rev. D* **72** (2005) 103517 [arXiv:astro-ph/0509565].